Available online at www.sciencedirect.com
ScienceDirect
Geochimica et Cosmochimica Acta 73 (2009) 2347–2365
Geochimica et Cosmochimica Acta
www.elsevier.com/locate/gca

Apatite (U–Th)/He thermochronometry using a radiation damage accumulation and annealing model

Rebecca M. Flowers [a,*], Richard A. Ketcham [b], David L. Shuster [c], Kenneth A. Farley [d]

[a] Department of Geological Sciences, University of Colorado at Boulder, 2200 Colorado Ave., UCB 399, Boulder, CO 80309, USA
[b] Department of Geological Sciences, Jackson School of Geosciences, University of Texas at Austin, Austin, TX 78712, USA
[c] Berkeley Geochronology Center, 2455 Ridge Road, Berkeley, CA 94709, USA
[d] Department of Geological and Planetary Sciences, California Institute of Technology, MS 170-25, Pasadena, CA 91125, USA

Received 13 October 2008; accepted in revised form 21 January 2009; available online 11 March 2009

Abstract

Helium diffusion from apatite is a sensitive function of the volume fraction of radiation damage to the crystal, a quantity that varies over the lifetime of the apatite. Using recently published laboratory data we develop and investigate a new kinetic model, the radiation damage accumulation and annealing model (RDAAM), that adopts the effective fission-track density as a proxy for accumulated radiation damage. This proxy incorporates creation of crystal damage proportional to α-production from U and Th decay, and the elimination of that damage governed by the kinetics of fission-track annealing. The RDAAM is a version of the helium trapping model (HeTM; Shuster D. L., Flowers R. M. and Farley K. A. (2006) The influence of natural radiation damage on helium diffusion kinetics in apatite. *Earth Planet. Sci. Lett.* **249**, 148–161), calibrated by helium diffusion data in natural and partially annealed apatites. The chief limitation of the HeTM, now addressed by RDAAM, is its use of He concentration as the radiation damage proxy for circumstances in which radiation damage and He are not accumulated and lost proportionately from the crystal.

By incorporating the RDAAM into the HeFTy computer program, we explore its implications for apatite (U–Th)/He thermochronometry. We show how (U–Th)/He dates predicted from the model are sensitive to both effective U concentration (eU) and details of the temperature history. The RDAAM predicts an effective He closure temperature of 62 °C for a 28 ppm eU apatite of 60 μm radius that experienced a 10 °C/Ma monotonic cooling rate; this is 8 °C lower than the 70 °C effective closure temperature predicted using commonly assumed Durango diffusion kinetics. Use of the RDAAM is most important for accurate interpretation of (U–Th)/He data for apatite suites that experienced moderate to slow monotonic cooling (1–0.1 °C/Ma), prolonged residence in the helium partial retention zone, or a duration at temperatures appropriate for radiation damage accumulation followed by reheating and partial helium loss. Under common circumstances the RDAAM predicts (U–Th)/He dates that are older, sometimes much older, than corresponding fission-track dates. Nonlinear positive correlations between apatite (U–Th)/He date and eU in apatites subjected to the same temperature history are a diagnostic signature of the RDAAM for many but not all thermal histories.

Observed date-eU correlations in four different localities can be explained with the RDAAM using geologically reasonable thermal histories consistent with independent fission-track datasets. The existence of date-eU correlations not only supports a radiation damage based kinetic model, but can significantly limit the range of acceptable time-temperature paths that account for the data. In contrast, these datasets are inexplicable using the Durango diffusion model. The RDAAM helps reconcile enigmatic data in which apatite (U–Th)/He dates are older than expected using the Durango model when compared with ther-

* Corresponding author.
E-mail address: rebecca.flowers@colorado.edu (R.M. Flowers).

0016-7037/$ - see front matter
doi:10.1016/j.gca.2009.01.015

mal histories based on apatite fission-track data or other geological constraints. It also has the potential to explain at least some cases in which (U–Th)/He dates are actually older than the corresponding fission-track dates.

1. INTRODUCTION

Accurate interpretation of (U–Th)/He thermochronometry data from an increasingly wide range of geologic settings depends on a complete understanding of He mobility in apatite. Early work sought to constrain He diffusivity as a function of temperature using a few model apatite specimens (Zeitler et al., 1987; Wolf et al., 1996; Warnock et al., 1997; Farley, 2000). These studies showed that He diffusion varies with grain-size but provided no compelling evidence that other factors, such as chemical composition, were important. Based on these data many workers adopted the high quality helium diffusion kinetic data (activation energy, frequency factor) available on the gem-quality apatite from Durango, Mexico (Farley, 2000), to interpret cooling histories from apatite (U–Th)/He dates. These kinetic data implied a He closure temperature of ~70 °C for an apatite of 70 μm radius assuming a cooling rate of 10 °C/Ma.

Based on a much wider set of observations, more recent work has suggested that radiation damage associated with U and Th decay causes an apatite's He diffusion parameters and thus closure temperature to evolve through time (Shuster et al., 2006). Unlike highly radiation-damaged zircons and titanites which rapidly lose He (Hurley, 1952; Damon and Kulp, 1957), Shuster et al. (2006) found that radiation damage at typical levels impedes He mobility. This was attributed to the formation of energy wells or traps from which He atoms must escape prior to diffusion through the intervening pristine, undamaged crystal structure. In the absence of a direct radiation damage proxy, a predictive kinetic model was developed in which the volume fraction of these α-decay-induced traps was assumed to be proportional to α particle (He) concentration. This model (the He trapping model, or HeTM) predicts that at temperatures low enough for radiation damage to accumulate, an apatite with higher eU (effective uranium concentration, a parameter that weights the decay of the two parents for their alpha productivity, computed as $[U] + 0.235 \times [Th]$) will accumulate more damage traps and will develop a higher He closure temperature than an apatite with lower eU that accumulates fewer damage traps.

The effect of radiation damage on He diffusion is quite large, corresponding to tens of degrees variation in closure temperature across the range of typical apatite eU. Thus for many time-temperature paths the HeTM yields (U–Th)/He dates very different from those predicted from Durango kinetics (Shuster et al., 2006). In addition, for certain thermal histories, the effects of radiation damage are manifested as a positive correlation between (U–Th)/He date and eU (Shuster et al., 2006; Flowers et al., 2007). This phenomenon can be exploited to obtain additional constraints on thermal histories by targeting apatites with a span of eU and an associated span of closure temperatures. This approach has analogs in the use of date-grain-size correlations in (U–Th)/He data (Reiners and Farley, 2001) and also F/Cl-date correlations in fission-track data sets (e.g., Green et al., 1986). Sample suites from the Colorado Plateau (Flowers et al., 2007, 2008) and the Canadian Shield (Flowers, 2009) display date-eU correlations that can be explained by the effects of radiation damage on He retentivity, and demonstrate the utility of this effect for thermal history interpretation. In this manuscript, we use "date" to refer to a model prediction or analytical result, and "age" to refer to the geological interpretation of a date.

New laboratory diffusion and annealing experiments confirm that the addition of radiation damage increases an apatite's closure temperature, and that thermal annealing of the damage reverses this effect (Shuster and Farley, 2009). These new data both corroborate the Shuster et al. (2006) trapping model, and provide a quantitative basis for further refining it. The major shortcoming of the He proxy for radiation damage in the HeTM is that under some circumstances radiation damage and He will not accumulate proportionately. For example, damage may accumulate in apatite at temperatures at which He is lost from the crystal. Similarly, damage may anneal at a rate different from that at which He is lost. Here, we develop a new kinetic model, the radiation damage accumulation and annealing model (RDAAM), that accounts for the evolution of apatite He diffusivity in response to both damage accumulation and annealing. We incorporate this new kinetic model into the HeFTy computer program (Ketcham, 2005), and assess the RDAAM's implications for the interpretation of apatite (U–Th)/He thermochronometry data. These simulations reveal that under common circumstances, damage accumulation and annealing can yield far older (U–Th)/He dates than previously expected, can produce distinctive correlations between He date and eU, and can cause He dates to be older than corresponding apatite fission-track (AFT) dates.

2. INFLUENCE OF RADIATION DAMAGE AND THERMAL ANNEALING ON APATITE HE DIFFUSION KINETICS

Shuster and Farley (2009) described experiments in which radiation damage was introduced into apatites by exposing them to high neutron fluences in a nuclear reactor as an analog for U and Th decay. In all samples the two helium diffusion parameters (E_a and D_o/a^2) increased, yielding large increases in T_c. These experimental results unambiguously demonstrate that the amount of radiation damage in an apatite crystal strongly influences its helium diffusion kinetics. The experiments also preclude the possibility that the ^{4}He concentration, [^{4}He], itself controls diffusivity,

which remained a potential explanation of the original T_c versus log([^{4}He]) correlation observed by Shuster et al. (2006).

In another series of experiments, Shuster and Farley (2009) demonstrated that thermal annealing above 290 °C for >1 h causes the opposite effect of neutron irradiation, specifically a decrease in E_a, D_o/a^2 and closure temperature Like the neutron-irradiated samples, the diffusion parameters of annealed apatites plot on the same $E_a - \ln(D_o/a^2)$ array as untreated natural samples, suggesting that annealing is simply undoing the consequences of damage accumulation in terms of He diffusivity. Here, we consider annealing to be the process by which atoms are re-ordered into a crystalline state from a disordered state.

These experiments showed that He diffusivity in apatite responds to the annealing of radiation damage as predicted by the kinetics of a fission-track annealing model (Shuster and Farley (2009), reproduced in slightly different form in Fig. 1). While this provides *prima facie* evidence that fission tracks are the damage that controls He diffusion, an alternative and equally valid explanation is that α decay damage from parent recoil and/or the α particle itself anneals with the same kinetics as fission damage. We are unaware of any general theory or observational data comparing the kinetics of annealing of the various damage types in apatite. Nevertheless the source of relevant damage can be important for our modeling because, while U and Th both produce α decay damage, only ^{238}U undergoes spontaneous fission. In particular, if α decay dominates the relevant radiation damage budget, then the important variable is eU concentration. Conversely, if fission damage dominates, then U concentration is the controlling variable. However, even this distinction may only have practical importance for thermal history analysis when the Th/U ratio is significantly different than the mean value for the apatites used in this study (0.9, excluding Durango).

Two simple observations support the conclusion that α decay rather than fission is the dominant source of damage controlling He diffusion. First, fission is an extraordinarily rare decay mode—the decay of ^{238}U yields just one fission event per 1.5×10^7 α particles. If fission tracks dominate the diffusion-relevant damage budget, either they are vastly more efficient at trapping He or they are far better preserved over geologic time than α decay damage. Second, Durango apatite has He diffusivity in excellent agreement with other apatites of comparable He concentration (Shuster et al., 2006). This is significant because Durango has a very unusual U/Th (and therefore U/eU) ratio—an order-of-magnitude lower than almost all apatites investigated by Shuster et al. (2006). This means that it has a comparably unusual and low ratio of fission to α decays. If fission damage dominated the He diffusivity behavior, one would expect it to have an anomalous and lower He closure temperature than observed for its He concentration relative to other apatites.

A more quantitative analysis of existing diffusion data further supports this conclusion. The irradiation experiments of Shuster and Farley (2009) indicate that neutron-induced damage is a good analog for the damage that controls He diffusion in nature. Furthermore, they observed a strong correlation between enhancement of an apatite's He retentivity and kerma—the kinetic energy absorbed during irradiation and an order-of-magnitude estimate of radiation damage introduced into the apatite. For example,

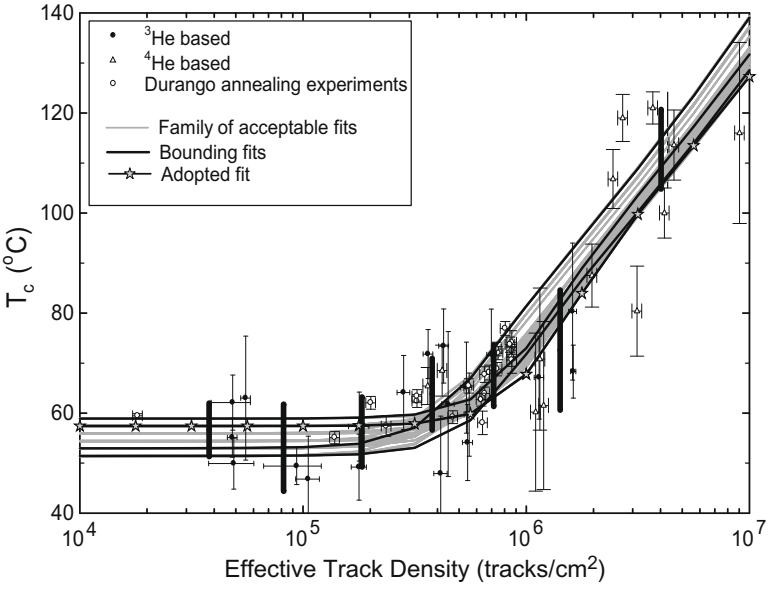

Fig. 1. Relationship between He closure temperature and effective fission-track density. Symbols are for data in Table EA-1 and distinguish which isotope was used as the diffusant. Only ^{4}He was used for the Durango annealing experiments. Vertical black bars indicate bin average targets for fitting (see text for details). Gray curves indicate predictions for various parameter sets that reasonably match the data in this figure and simultaneously in Figs. EA-1 and EA-2. Black curves are those which bound the range of acceptable fits and for which the parameter values are listed in Table 1. Black curve with stars indicates results for the parameter set used in the modeling section.

$\sim 10^{16}$ MeV/g of kerma causes an initially damage-free apatite to increase in T_c by ~30 °C.

The correlation between He concentration and He closure temperature (Shuster et al., 2006) permits a similar computation for apatites damaged by U and Th decay in nature. The same increase in He retentivity of 30 °C in an initially low damage apatite is correlated with an increase of ~30 nmol/g of α particles. The associated kerma is $\sim 10^{17}$ MeV/g, of which $\sim 10^{15}$ MeV/g is attributable to α recoil. Regardless of whether the relevant damage is produced by α recoils alone, or both recoils and α particles, the energy associated with the damage is consistent with the neutron results to within an order-of-magnitude. In contrast, the kerma associated with fission decay is far lower. If this 30 nmol/g of ^{4}He is solely from ^{238}U decay, then the number of fission events is $\sim 1.2 \times 10^9$/g. With a mean energy of ~200 MeV per fission, this corresponds to a kerma of $\sim 10^{11}$ MeV/g. This is 5 orders of magnitude lower than observed in the neutron case. Thus fission damage would need to be 4–6 orders of magnitude more efficient (per MeV/g of kerma) than α decay and neutron damage in order to dominate He retentivity. Although there are differences among these various damage sources (e.g., in terms of how interconnected the damage is, Fleischer, 2003), it is hard to see why they would lead to such a dramatic difference in helium migration behavior.

Taking these observations together we believe it is most reasonable to assume that α decay damage is the major factor that controls He diffusion in apatite, and that this damage anneals with kinetics similar to fission-track annealing.

3. RADIATION DAMAGE ACCUMULATION AND ANNEALING MODEL (RDAAM)

3.1. Overview and database

Shuster et al. (2006) developed an equation to describe He diffusion kinetics in which ^{4}He concentration was used as a measure of the volume fraction of radiation damage. This formulation is sensible for apatites which accumulate but do not anneal damage and which do not lose He by diffusion because under such circumstances crystal damage from U and Th decay will be very strongly correlated with the associated production of a ^{4}He nucleus. However a more generally applicable proxy for radiation damage is desirable. The ideal proxy would be both readily measurable to allow calibration of the model and easily predicted in forward models to allow computation of apatite (U–Th)/He dates on arbitrary time-temperature paths. While fission-track length reduction correlates with decreasing He retention in the annealing experiments of Shuster and Farley (2009), this measure is not robust for a general application because track lengths alone do not accurately document *volume fraction* of radiation damage. For example, in the absence of annealing, all fission tracks will have the same length regardless of how many of them there are. Similarly fission tracks within a given sample may have a range of lengths rather than a single length.

Here we explore and ultimately adopt *effective spontaneous fission-track density* as an alternative proxy for radiation damage. Spontaneous fission-track density (ρ_s) is the number density of natural fission tracks observed on a polished apatite surface after etching, commonly reported in tracks/cm^2. By analogy to effective Uranium concentration (eU), *effective* spontaneous fission-track density ($e\rho_s$) is a measure of radiation damage that incorporates contributions from both U and Th decay in proportion to α productivity (see Electronic annex). Note that this proxy does not require or imply that the relevant damage for He diffusion is fission tracks—$e\rho_s$ is simply used as a proxy for *total* radiation damage and its annealing. The main reason for adopting $e\rho_s$ is that it is easily measured on apatites and models exist to predict it in apatites on specified time-temperature paths.

Following Shuster et al. (2006), we seek a quantitative expression for the kinetic parameters governing He diffusion in apatite as a function of temperature and a radiation damage proxy (in this case $e\rho_s$). The new *radiation damage accumulation and annealing model* was developed and calibrated using the same data set used by Shuster et al. (2006) for the HeTM: He diffusion kinetic data obtained on natural samples in the laboratory. These data and their sources are described in Electronic annex and are listed in Table EA-1. For all 33 samples in the database we measured fission-track density or obtained it from published or unpublished sources. In addition to the natural apatites, the database also includes data for 22 partially annealed aliquots of Durango apatite from Shuster and Farley (2009). These samples are important for assessing how He diffusion responds to radiation damage annealing—information that cannot easily be obtained from untreated natural samples. For these samples fission-track densities were computed using the fission-track annealing model of Ketcham et al. (2007). Details of the conversion from fission-track density to $e\rho_s$, including the effects of proton-induced damage in some of the samples, are given in Electronic annex.

3.2. Functional form of the RDAAM

Fig. 1 and Electronic annex Figs. EA-1 to EA-3 show the relationship between $e\rho_s$ and observed He diffusion characteristics including closure temperature (computed for a cooling rate of 10 °C/Ma) from the data in Table EA-1. In general the relationships are quite similar to those reported by Shuster et al. (2006) when correlating against [^{4}He]. Most notable is the roughly log-linear relationship between the damage proxy and closure temperature, a relationship predicted if radiation damage acts as a He trap (Shuster et al., 2006). Conversion from [^{4}He] to $e\rho_s$ as damage proxy allows the annealed Durango samples to be included on these figures; importantly, these aliquots plot in the same general region as samples never subjected to laboratory annealing. These observations justify the use of $e\rho_s$ as a proxy for the volume fraction of radiation damage in the samples, both during damage accumulation and during damage annealing.

The equation derived by Shuster et al. (2006) relating the volume fraction of radiation damage to He diffusivity has the form:

$$\frac{D(T,{}^4\mathrm{He})}{a^2} = \frac{\frac{D_{oL}}{a^2}\cdot e^{\frac{-E_L}{RT}}}{\left(k_o\cdot v_{rd}\cdot e^{\frac{E_{trap}}{RT}}\right)+1} \quad (1)$$

Here D/a^2 is the helium diffusivity normalized to the grain radius (a), ^{4}He is the He concentration, E_{trap} is the activation energy associated with the radiation damage traps, R is the gas constant, and T the Kelvin temperature. In a slight modification of the terminology of Shuster et al. (2006), we use D_{oL} and E_L to refer to the diffusivity at infinite temperature and the activation energy of He diffusion through the undamaged crystal. This is to distinguish these quantities from those obtained empirically from regression of a diffusion Arrhenius plot, conventionally denoted D_o/a^2 and E_a.

The term $k_o v_{rd}$ is the product of radiation damage density (v_{rd}) and a scaling factor (k_o). Based on observed correlations between [^{4}He] and He diffusivity similar to those in Figs. 1 and Figs. EA-1 to EA-3, Shuster et al. (2006) suggested that $k_o v_{rd}$ could be replaced by the quantity Ψ [^{4}He] where Ψ is an empirical scaling factor. Here we wish to replace Ψ [^{4}He] with a function of $e\rho_s$.

To assess how well a given function of $e\rho_s$ accounts for the observations, we followed the same procedure as Shuster et al. (2006): we generated using Eq. (1) synthetic Arrhenius plots for each sample in Table EA-1 in the temperature range 200–275 °C, assuming values for the unknown parameters (D_{oL}, E_L, E_{trap} and the new scaling factor Ψ_ρ) and using $e\rho_s$ of the given sample. From regression of these Arrhenius plots we obtained D_o/a^2, E_a, and closure temperature to be compared with laboratory observations.

Initially we replaced Ψ [^{4}He] with $\Psi_\rho\, e\rho_s$ (i.e., a relationship linear in $e\rho_s$) and attempted to fit the four unknown parameters to the T_c vs $e\rho_s$ data (Fig. 1). However it became apparent that no parameter combination could simultaneously account for both the low damage and high damage end of the sample spectrum—the data show far more curvature than this linear model allows. Inspection of the fits obtained by Shuster et al. (2006) using ^{4}He as the independent variable show the same effect. To verify the high T_c values in highly damaged apatites, we analyzed three new samples with $e\rho_s > 2$ million/cm^2. As shown in Table EA-1, all three gave $T_c > 100$ °C, confirming the more limited earlier data. Our model needs to honor these high T_c samples.

In the absence of a theoretical understanding of how the damage density relevant to He diffusion should scale with $e\rho_s$, we here adopt an empirical approach. By inspection, adequate fits are obtained by replacing Ψ [^{4}He] with $(\Psi_\rho e\rho_s + \Omega_\rho e\rho_s{}^3)$ where both Ψ_ρ and Ω_ρ are empirical constants. Further work is required to establish whether this functional form has any physical significance, or if other forms are more appropriate.

3.3. Quantitative fitting

We have a variety of observations we wish to simultaneously fit. The most sensitive are a) the linear relationship between E_a and $\ln(D_o/a^2)$ as highlighted by Shuster and Farley (2009) and present in samples with low damage density ($e\rho_s < 1$ million/cm^2) (Fig. S1), and b) the correlations between $e\rho_s$ vs. E_a and $e\rho_s$ vs. T_c (Figs. 1 and EA-2). The correlation between $e\rho_s$ and $\ln(D_o/a^2)$ is neither strong (Fig. EA-3), nor, given the three fitting targets outlined in (a) and (b), unique. We therefore do not consider it further.

To simultaneously honor these considerations, we did the following (in this order):

1. We divided the data set in Table EA-1 into 7 bins of equal size in $\log(e\rho_s)$ and averaged all data within the bins. This prevents the very high sample abundance in some parts of the plots from completely dominating the fits. Figs. 1 and EA-2 show these averages, plotted at the average value of $e\rho_s$ of the samples in the bin. The uncertainties are the standard deviation of the values within each bin. The Tioga sample is such a flier that it was excluded from this computation.
2. By inspection the lower limit on E_a for a sample is given by E_L in Equation (1). In our sample suite there are a substantial number of samples (5) with $E_a < 122.3$ kJ/mol. Thus we require that $E_L \leqslant 122.3$ kJ/mol. The correlation between E_a and $\ln(D_o/a^2)$ among the low damage samples (Fig. EA-1) along with their T_c range further limit E_L and $\ln(D_{oL}/a^2)$. By comparison to the bin averages we determine that E_L values lower than 119 kJ/mol cannot simultaneously yield the linear relationship between E_a and $\ln(D_o/a^2)$ and the appropriate range of values for T_c in the two lowest damage bins. This constrains $119 < E_L < 122.3$ kJ/mol. This range simultaneously restricts $\ln(D_{oL}/a^2)$ to lie between 9.3 and 10.6.
3. Parameter space was searched for combinations that yielded curves that passed through at least 12 of the 14 means for E_a vs $e\rho_s$ and for T_c vs $e\rho_s$; this "success rate" of 12/14 was selected arbitrarily to permit a diversity of fits that reasonably accommodate the data. The space for E_a and $\ln(D_o/a^2)$ was restricted to the values found in step 2. The other parameters were allowed to range widely. The only restriction on them was that Ψ_ρ was required to be $\geqslant 9$ orders of magnitude larger than Ω_ρ. Smaller values of Ψ_ρ have no influence on the result; i.e., the term $\Psi_\rho\, e\rho_s$ becomes negligible compared to $\Omega_\rho\, e\rho_s{}^3$. The resulting family of acceptable fits is shown in Figs. 1 and EA-1 to EA-3 as gray lines.

It is obvious from an inspection of Figs. 1 and EA-1 to EA-3 that while our model captures the general behavior of the data, no single parameter set can accommodate all of it within error. The "acceptable" fit parameters are at best a compromise and likely hide additional complexity in the controls on He diffusion or unrecognized errors in the measured quantities. We consider the match to T_c to be both the most convincing, and for our purposes, the most relevant. For calibration of our model the closure temperature, rather than the particular combination of parameters by which it is achieved, is most critical. This is because multiple combinations of parameters can yield the same diffusivity through the range of partial He retention, and so will yield very similar T_c. The closure temperature is a single parameter which most simply describes the helium diffusion kinetics and absolute diffusivity at relevant temperatures.

Table 1
Representative acceptable fit parameters. Parameter set 2 (bold) was used for the modeling in Section 5. Ω_ρ and Ψ_ρ assume $e\rho_s$ is in units of tracks/cm^2.

Parameter set	log (Ω_ρ)	log (Ψ_ρ)	E_{trap} (kJ/mol)	ln(D_{oL}/a^2) (ln(1/s))	E_L(kJ/mol)
1	−20.4	−10.8	25	10.167	121.2
2	**−22**	**−13**	**34**	**9.733**	**122.3**
3	−21.2	−11.4	29	9.517	122.3
4	−19.6	−9.8	22	9.95	121.2

To encompass some degree of imprecision, rather than select a single "best" parameter set, four sets of parameters were selected from those shown in Figs. 1 and EA-1 to EA-3. These parameter sets, listed in Table 1, essentially span the range of acceptable fits. Note that the curves associated with these parameter sets cross, e.g., in Fig. 1, so the relative order of dates obtained from them will depend on the time-temperature path and the eU being investigated. These four sets yield rather similar results for most paths we investigated and in general parameter set 2 yields results in the middle of the range (examples in Fig. EA-4). Thus for the purpose of illustration of the consequences of the RDAAM, we will use just this single parameter set.

Previous work has shown that in the case of Durango apatite, He diffusion scales with the inverse square of the physical grain-size (Farley, 2000). Similarly, in a least one data set, (U–Th)/He dates are observed to be older in larger grains than in coexisting smaller grains (Reiners and Farley, 2001). Both of these observations suggest that the He diffusion domain in apatite corresponds to the physical grain. However because we have not documented this to be true in the samples used for the calibration of the RDAAM, and because nearly all samples in the data set have a common grain-size (about 60 μm radius) we have chosen to be conservative and fit for D_{oL}/a^2 rather than for D_{oL} itself. This does not substantially impact the utility of our model because most apatites subjected to (U–Th)/He dating are of about this grain-size, and furthermore one can expressly accommodate the effect by adjusting the parameter D_{oL}/a^2 for a values that differ from 60 μm. The implementation of the RDAAM model in HeFTy includes this functionality.

4. INTEGRATION OF TRAP ANNEALING INTO THERMAL HISTORY MODELING

We now describe how we incorporate Eq. (1) into a model that computes (U–Th)/He dates given a thermal history and eU, as implemented in the HeFTy computer program (Ketcham, 2005). We use a hybrid of conventional fission-track annealing and helium diffusion computations, in which the fission-track calculation is used to characterize damage accumulation and annealing at all stages of the time-temperature path, which in turn is used to continuously influence diffusivity.

The calculations behind fission-track thermal modeling are described in detail by Ketcham (2005), but we summarize some of the concepts here. Fission tracks form continuously throughout a crystal's history, and immediately after formation they begin to anneal. Thus, the fission tracks present at any given time have a range of ages, and will have been annealed to different extents, which in turn will influence their contribution to the net fission-track density. The fission-track computation thus divides the thermal history into a set of increments and keeps track of the annealing extent of the tracks generated during each one. At any given stage of the thermal history, the accumulated fission-track damage is calculated as a weighted summation of contributions from all previous time steps.

For this study we use the fission-track annealing calibration of Ketcham et al. (2007). This model characterizes $r_{c,B2}$, the reduced mean length of fission tracks that form along the crystallographic **c** axis for highly-annealing-resistant apatite *B2* (Carlson et al., 1999), as:

$$r_{c,B2} = \left\{ \left[C_0 + C_1 \frac{\ln(t) - C_2}{\ln(1/T) - C_3} \right]^{1/\alpha} + 1 \right\}^{-1} \quad (2)$$

where α and C_0 through C_3 are fitted parameters (Ketcham et al., 2007, Table 5c, line 1). We use here the fission-track convention of "reduced" referring to a quantity that has been normalized by its unannealed equivalent, resulting in a dimensionless number reflecting proportion of annealing. The reduced mean **c**-axis-projected length of fission tracks in some less-resistant apatite, $r_{c,lr}$ is then obtained using:

$$r_{c,lr} = \left(\frac{r_{c,B2} - r_{mr0}}{1 - r_{mr0}} \right)^{\kappa} \quad (3)$$

where r_{mr0} and κ are fitted parameters required to relate any particular apatite variety to *B2* apatite. Although they are fitted as separate values, Ketcham et al. (2007) found that, in general, $r_{mr0} + \kappa \approx 1.04$, and this simplification is employed in HeFTy. Durango apatite is characterized by an r_{mr0} value of 0.79, whereas typical F-apatite has r_{mr0} values from 0.81 to 0.83. Reduced length ($r_{c,lr}$) is then converted to reduced spontaneous density (ρ_r) using the empirical length-density conversion provided by Ketcham et al. (2003):

$$\rho_r = 1.600 r_c - 0.600, \quad r_c \geqslant 0.765;$$
$$\rho_r = 9.205 r_c^2 - 9.157 r_c + 2.269, \quad r_c < 0.765 \quad (4)$$

The annealing calculation provides the dimensionless reduced spontaneous density of fission tracks attributable to each model time step. For fission-track modeling, these are combined with the duration of each time step to determine each time step's contribution to the total age, and there is no reason to calculate a non-reduced density. However, because the RDAAM model uses measured spontaneous fission-track density (ρ_s; observed tracks/cm^2) such a conversion is required, and so we describe the necessary conversion in detail here. Spontaneous track density is traditionally characterized as:

$$\rho_s = \frac{\lambda_f}{\lambda_D}\rho_v \eta L \quad (5)$$

Where λ_f and λ_D are the fission-track and total decay constants, respectively, ρ_v is the volume density (tracks/cm^3) of daughter products (or, less ambiguously, parents that have undergone decay), η is the fission-track etching efficiency of apatite (dimensionless), and L is the etchable range of a single fission fragment, which is equal to half the total etchable fission-track length (~8.1 μm for an unannealed track). Jonckheere and Van den Haute (1996) documented that the assumptions concerning etching leading to calculation of η were oversimplified, and moreover ignored the subjectivity of the operator in recognizing tracks, which is summarized as the variable q whose effects cannot be separated from η. Jonckheere and Van den Haute (2002) measure ηq for Durango apatite to be 0.91 ± 0.01. Although there is not yet an agreed-upon value for λ_f due to difficulties in measuring it, the value of 8.46×10^{-17} yr^{-1} (Galliker et al., 1970) has been shown by Jonckheere (2003) to yield a correct age for Durango apatite when used in the context of an absolute dating approach.

When considering the component of fission-track density formed during any time interval (t_1, t_2) due to decay of ^{238}U (expressed in atoms/volume), ρ_v is calculated as:

$$\rho_v = \left[^{238}\mathrm{U}\right]\left(e^{\lambda_{238}t_2} - e^{\lambda_{238}t_1}\right) \quad (6)$$

where λ_D has been replaced by λ_{238} to keep track of which isotope is decaying. The previous two equations provide a reasonable estimate of ρ_s. Characterization of total α decay damage requires including appropriate contributions for other isotopes (i.e., $e\rho_s$). Assuming that the contribution from each parent isotope is proportional to the number of α particles it produces, ρ_v becomes:

$$\rho_v = \frac{8}{8}\left[^{238}\mathrm{U}\right]\left(e^{\lambda_{238}t_2} - e^{\lambda_{238}t_1}\right) + \frac{7}{8}\left[^{235}\mathrm{U}\right]\left(e^{\lambda_{235}t_2} - e^{\lambda_{235}t_1}\right) + \frac{6}{8}\left[^{232}\mathrm{Th}\right]\left(e^{\lambda_{232}t_2} - e^{\lambda_{232}t_1}\right) \quad (7)$$

Although Sm can also make a small contribution to damage density, its low contribution to total alpha decays in virtually all natural cases compounded by the comparatively low energy of its alpha particle (and thus resultant damage) led us to omit it here.

The effect of annealing in the traditional density equation is to reduce L, reflecting the fact that the probability of a track intersecting an internal plane for ρ_s measurement falls proportionately with its length. However, the strong anisotropy of fission-track annealing in apatite requires an expansion of this concept, as low-**c**-axis-angle tracks will persist after high-angle tracks have annealed entirely (Ketcham, 2003). As a result, the appropriate correction factor is density-based, rather than length-based. Thus, we leave L at its unannealed value and instead multiply the spontaneous density equation by ρ_r, as calculated above, to incorporate the effect of annealing.

To summarize, we calculate $e\rho_s$ for damage formed in a single time step bounded by times t_1 and t_2 as:

$$e\rho_s(t_1, t_2) = \frac{\lambda_f}{\lambda_D}\rho_v(t, \mathrm{U}, \mathrm{Th})\eta q L \rho_r(t, T) \quad (8)$$

where ρ_v, reflecting track generation, is calculated from Eq. (7) and ρ_r, reflecting track annealing, is defined by Eqs. (2)–(4). These equations provide a way to relate the observed parameters shown in Fig. 1 to the kinetics of fission-track annealing that have been calibrated with 20 years of experimental results.

The final stage of the calculation is simply to sum the density contributions from all time steps prior to the one in which diffusivity is being calculated. Because damage retention always begins at least as early as He retention, the computation can proceed in two discrete stages. First, the state of radiation damage at all times during the modeled history is calculated, which then provides input for subsequent He diffusion calculations. It bears noting that, because radiation damage is retained at higher temperatures than He is retained, a substantial portion of the thermal history influencing He diffusivity may precede any He accumulation.

A number of underlying assumptions inherent to fission-track modeling are also worth stating explicitly. First, we assume that annealing is independent of damage density. All damage zones created at the same time will anneal the same amount given a certain thermal input regardless of how many there are; there is no provision, for example, for overlapping damage zones. A linked assumption is that all of the damage due to a single atom's decay series occurs at the time of the decay of the head-of-chain parent (^{238}U, ^{235}U, ^{232}Th). This is certainly an adequate simplification for typical geological time-scale modeling. Finally, we use the assumption employed for fission tracks that damage annealing can be treated as an "equivalent time" process: the state of a trap at a given extent of annealing is independent of the particular time-temperature history that brought it about.

5. IMPLICATIONS OF THE RDAAM FOR APATITE HE THERMOCHRONOMETRY

The RDAAM differs from the original He-based trapping model of Shuster et al. (2006) in that effective fission-track density, rather than [^{4}He], is used as the proxy for radiation damage. For temperature histories in which radiation damage and He begin accumulating simultaneously and neither annealing nor diffusive He loss occur, the HeTM and the RDAAM should be equivalent because $e\rho_s$ and [^{4}He] increase in fixed proportion. The only difference between them arises from the slightly different calibration data sets used and the use of a nonlinear function of the radiation damage proxy in the RDAAM. However, for most thermal histories involving He loss and/or annealing, the RDAAM is expected to predict higher retentivities and older dates than those predicted by the HeTM. This is because while both models include the disappearance of traps, in general the fission-track proxy requires higher temperatures than the He proxy to induce the same degree of trap disappearance. Both of these models fundamentally differ from Durango diffusion kinetics (the "Durango model") because the apatite He retentivity evolves through time rather than being invariant. Thus, apatite suites characterized by a span of eU may develop a span of retentivities

and associated closure temperatures. Fortuitously Durango apatite has a He age and eU value that is in the middle of the calibration data set, so we expect that in some cases the RDAAM will yield younger dates than the Durango model, and in some cases older dates.

In this section we use HeFTy to compare the predictions of the RDAAM with those of the conventional Durango model for common thermal histories. We used six different eU values ranging from 4 to 150 ppm to illustrate the sensitivity of the model. This range in eU encompasses ~95% of the observed range in ~3500 apatite (U–Th)/He analyses acquired in the Caltech lab over the last few years. The median eU in that suite is 28 ppm, which we refer to below as the value for "typical apatite". We adopt an equivalent spherical radius of 60 μm for all simulations, as this is a common grain-size of apatites analyzed for (U–Th)/He dating. All models also include the effect of alpha-ejection for this grain-size. The grain-size influence on (U–Th)/He ages for some thermal histories is a well-recognized phenomenon (Reiners and Farley, 2001), and below we compare the magnitudes of the grain-size and eU effects in several time-temperature simulations. We assume a surface temperature of 0 °C for the generic simulations, as varying the surface temperature from 0 to 15 °C has a negligible effect on the simulated dates.

Apatites are characterized by differing resistance to fission-track annealing over geological time scales, depending in part on Cl and OH content, as well as less common cation substitutions. As described previously, HeFTy uses the r_{mr0} value to quantify the kinetic annealing behavior of apatite (Ketcham et al., 1999). We assume that the resistance of damage to annealing may in turn exert a secondary control on the apatite He retentivity, and for this reason the r_{mr0} value is specified by the user in the RDAAM. An r_{mr0} value of 0.83 is representative of a fluorapatite with a typical annealing resistance. An r_{mr0} value of 0.79 is appropriate for Durango, and represents an apatite with greater resistance to fission-track annealing than an apatite of typical composition. Varying the r_{mr0} value used in the RDAAM from 0.79 to 0.83 has an insignificant effect on most results. We used the Durango r_{mr0} value of 0.79 for the generic RDAAM and AFT thermal history simulations so that we maintain internal consistency when comparing the results with the Durango model. For all the fission-track simulations below, we used the annealing model of Ketcham et al. (2007).

Below we also explore examples of (U–Th)/He datasets that have patterns that are consistent with predictions of the RDAAM. We simulated these data using the inverse modeling capabilities of the HeFTy program. In these inverse modeling simulations, time-temperature constraints were specified (described in the text and indicated on the figures), and 10,000 random thermal histories satisfying these constraints were generated and resulting dates compared against observations. These inversions seek time-temperature paths that simultaneously accommodate the sample dates and their associated eU values. The results are shown as path envelopes encompassing the time-temperature histories that generated "good" and "acceptable" fits to the data. Refer to Ketcham (2005) for further details regarding inverse modeling and statistically significant data fits in HeFTy. These simulations used the mean equivalent spherical radius of apatites analyzed in the sample and a representative apatite r_{mr0} value of 0.83.

5.1. Monotonic cooling

5.1.1. Characteristics of monotonically cooled apatite suites

We first consider constant monotonic cooling histories that begin at a temperature of 120 °C, above the temperature for retention of both He and radiation damage, and end at 0 °C. We computed an "effective closure temperature", T_{ec}, by determining the temperature associated with the simulated (U–Th)/He date at that time in the past, consistent with the definition of "closure temperature" by Dodson (1973). Fig. 2 depicts T_{ec} as a function of cooling rate and eU as predicted by the RDAAM. There are two key results apparent in the figure. First, the greater buildup of radiation damage in higher eU apatites causes them to have higher T_{ec} than lower eU apatites at all rates of cooling. At a cooling rate of 1 °C/Ma the closure temperatures range from 46 to 77 °C as eU is increased from 4 to 150 ppm. Second, while the Dodson (1973) formulation for closure temperature predicts that T_c values decrease at slower cooling rates, the RDAAM predicts that T_{ec} values actually *increase* with slower cooling. For a 28 ppm eU apatite, the T_{ec} value first decreases as cooling rates are reduced below 10 °C/Ma, reaches a minimum value at ~ 2 °C/Ma, then increases again. The cooling rate at which T_{ec} is a minimum increases with eU: it occurs at ~0.5 °C/Ma for a 4 ppm eU apatite, and at ~ 5 °C/Ma for a 150 ppm eU apatite. These patterns together reflect the fact that at slower cooling rates, an apatite has more time to accumulate radiation damage that retards He diffusion, and the higher the eU

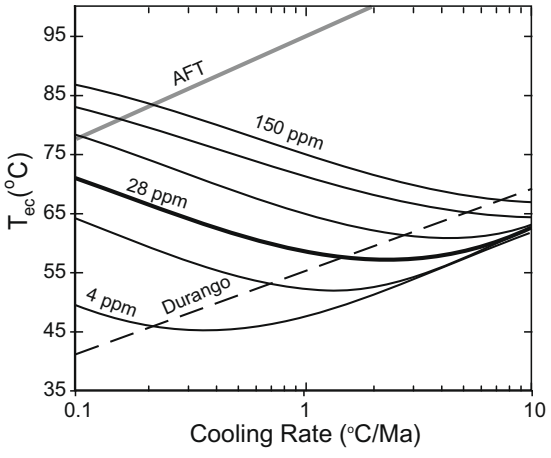

Fig. 2. Effective closure temperature as a function of cooling rate and eU computed using the RDAAM. The simulated thermal histories begin at 120 °C at different times in the past to yield the reported monotonic cooling rates. Solid black lines are for apatites with different eU values of 150, 100, 60, 15, and 4 ppm from top to bottom. Solid bold line is for typical eU value of 28 ppm. Results for conventional Durango diffusion kinetics (dashed black line) and the apatite fission-track system (solid gray line) using the annealing model of Ketcham et al. (2007) are also shown.

value, the more significant is the effect. An increase in T_{ec} values at slower rates of cooling was not predicted by the HeTM, because in this model the apatite [He] rather than fission-track density was used as the proxy for radiation damage. During passage through the zone of partial He retention the diffusive loss of He from the crystal is greater than the annealing of radiation damage, such that the HeTM predicts a smaller increase in He retentivity than the RDAAM.

Several additional features of the RDAAM are revealed by comparison with predictions of the Durango model and the AFT system. At fast cooling rates (~8–10 °C/Ma), the RDAAM predicts lower T_{ec} values than the Durango model for all eU, because there is insufficient time during cooling for radiation damage to build up to the levels found in Durango apatite. For a 10 °C/Ma cooling rate, the RDAAM predicts that a 28 ppm eU apatite will have a T_{ec} value of 62 °C, or 8 °C lower than the Durango prediction of 70 °C. In contrast, at slow cooling rates (0.1–0.2 °C/Ma), the RDAAM predicts higher T_{ec} values than the Durango model for all eU values, owing to the longer time for radiation damage to accumulate and retard He diffusion. At 0.1 °C/Ma, the T_{ec} of a 28 ppm eU apatite is 71 °C, or 29 °C higher than predicted by the Durango model. For a 150 ppm eU apatite it is 86 °C, or 45 °C higher than predicted by the Durango model. As shown in Fig. 2, at these slow cooling rates, the RDAAM predicts that apatites with 60–150 ppm eU will have T_{ec} values equivalent to, or up to 9 °C higher than, the T_{ec} values for the AFT system. Thus, these apatites are predicted to yield (U–Th)/He dates older than their AFT dates. This is an important observation that we will flag repeatedly in the following simulations.

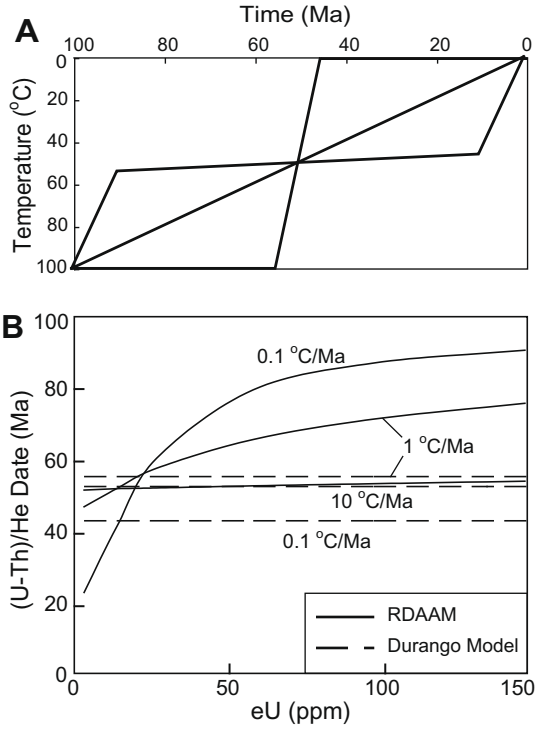

Fig. 3. (A) Simulated time-temperature paths characterized by 10, 1 and 0.1 °C/Ma cooling rates. (B) (U–Th)/He date as a function of eU for the thermal histories in (A) computed using the RDAAM (solid lines) and conventional Durango diffusion kinetics (dashed lines).

At slow cooling rates, the RDAAM predicts a positive correlation between (U–Th)/He date and eU, in contrast to the Durango model that necessarily predicts uniform dates. For example, Fig. 3 shows the results for histories involving cooling from 100 to 0 °C at rates of 10, 1 and 0.1 °C/Ma for some duration between 100 Ma and the present. These histories were selected arbitrarily to illustrate correlations between date and eU and how they relate to cooling rate. At fast cooling rates, the apatites yield uniform dates regardless of eU, because there is insufficient time for their He diffusivities to diverge during rapid cooling. At slower cooling rates, a positive but non linear correlation between date and eU develops, because apatites with higher eU accumulate more radiation damage, develop a higher T_{ec}, and yield older dates than apatites with lower eU. Thus, the presence or absence of an eU correlation in an apatite suite that underwent monotonic cooling can be used to constrain cooling rates, as illustrated by the dataset described in the next section.

5.1.2. A testable prediction and an example from a geological dataset

The RDAAM makes the testable prediction that at slow cooling rates, apatites characterized by a broad span of eU will yield a positive correlation between helium date and eU. Fig. 4A shows previously published data that display such a correlation for eight basement samples expected to share a common thermal history from the Upper Granite Gorge of the Grand Canyon (Flowers et al., 2008). Fig. 4B depicts the inverse modeling results of HeFTy for these samples using the RDAAM. The only thermal history constraints imposed in the HeFTy simulations are peak temperatures of 120 °C at 80 Ma, consistent with complete annealing of apatite fission tracks during Cretaceous time (Naeser et al., 1989; Dumitru et al., 1994; Kelley et al., 2001), and cooling to a 5 °C surface temperature by the present time. The best-fit models require ~30 Ma of slow cooling through temperatures of 70–45 °C. These results are similar to histories inferred previously for these samples using the HeTM (Flowers et al., 2008) and are compatible with the multiphase cooling history interpreted from AFT length data for basement samples from this same area (Kelley et al., 2001).

The large variations in date and eU in these eight samples could never be explained by the Durango model, and from a practical perspective they greatly restrict the acceptable time-temperature paths for the region. For example, Fig. 4C depicts the RDAAM inverse modeling results for the same thermal history constraints used in Fig. 4B, but using only the mean date of the four samples with eU values from 14 to 21 ppm. When the four higher and lower eU samples that define the eU correlation are excluded, a much wider range of permissible time-temperature paths are predicted.

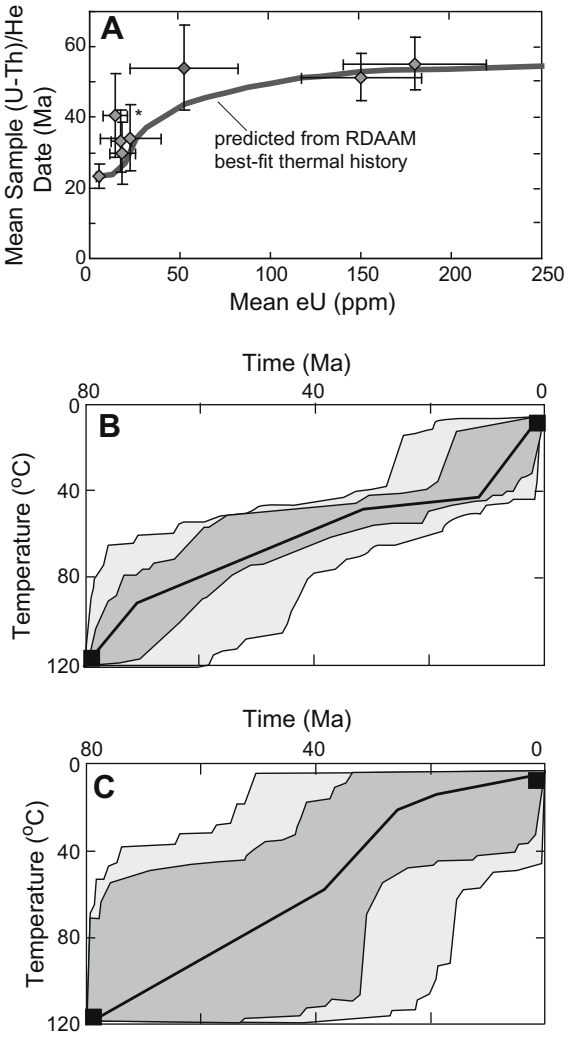

Fig. 4. (A) Apatite (U–Th)/He data from eight Grand Canyon crystalline basement samples plotted as mean sample apatite (U–Th)/He date versus mean sample apatite eU, from Flowers et al. (2008). The errors plotted are the 1-sigma standard deviation of the mean. Asterisk (*)-one aliquot excluded. The predicted date-eU correlation for the best-fit thermal history in (B) is shown as the solid gray line. (B) Inverse modeling results using the RDAAM in HeFTy. The full eU range is used in the simulation. The only constraints imposed on the thermal history are indicated by the two black squares at 80 and 0 Ma. The good-fit field of solutions is shown by the darker gray shading, and the acceptable-fit field in lighter gray shading. The solid black line represents the best-fit thermal history. The results agree well with independent geological and AFT constraints in the area. (C) Same as in (B), but simulations use only the mean date and mean eU value for the four intermediate eU samples, and exclude the higher and lower eU samples. A broader spectrum of thermal histories is permitted than in (B).

5.2. Helium partial retention zone

5.2.1. Characteristics of the HePRZ

The helium partial retention zone (PRZ) is the temperature range over which He dates change very rapidly, from near quantitative retention at low temperatures to extremely rapid loss at high temperatures (Wolf et al., 1998). It is operationally defined as the range of temperatures where He dates lie between 90% and 10% of the holding time assuming isothermal conditions. Fig. 5A shows the variations in date expected for apatites held isothermally for 75 m.y using both the RDAAM and the Durango model. Like the Durango model, the RDAAM predicts a characteristic sigmoidal shape for the PRZ at all eU. However, apatites with lower eU and less accumulated radiation damage have a lower He retentivity than apatites with higher eU, so the PRZ plots at increasingly higher temperatures with increasing eU. Where the RDAAM PRZ plots relative to the Durango PRZ depends on whether the simulated apatite contains more or less radiation damage (and thus is more or less retentive) than Durango apatite. From Fig. 5A it is clear that following the 75 Ma holding time, a 4 ppm eU apatite is less retentive than Durango, while apatites containing $\geqslant$28 ppm eU are more retentive. As we discuss in Section 5.2.2, this relative pattern evolves with holding time. The inset in Fig. 5A compares the influence of apatite grain-size (radius that varies from 35 to 100 μm for a 28 ppm eU apatite), with the influence of apatite eU (4–150 ppm eU variation for fixed apatite radius of 60 μm, gray shaded field) on the PRZ. The RDAAM predicts that the grain-size effect, although important, is secondary to the eU effect. For example, at 50 °C within the PRZ after the 75 Ma holding time, the grain-size effect yields a 26 Ma variation, and the eU effect a 61 Ma variation, in the (U–Th)/He date.

Like in the case of monotonic slow cooling, the RDAAM predicts a positive but nonlinear correlation between (U–Th)/He date and eU for apatites at a specific temperature within the PRZ (Fig. 5B). The magnitude of the effect is greatest in the center of the PRZ temperature window, where apatites spanning 4–150 ppm can nearly encompass the age range of the entire PRZ. In contrast, the Durango model predicts a uniform distribution of dates regardless of eU (Fig. 5C and D). Looked at differently, these same simulated dates indicate that it is possible for lower eU apatites at cooler temperatures within the PRZ to have younger dates than higher eU apatites at higher temperatures. In the example in Fig. 5B, a 15 ppm eU apatite at 40 °C has a date of 48 Ma, while a 150 ppm eU apatite at 60 °C has a date of 62 Ma. Thus, the RDAAM predicts that apatite dates need not systematically decrease with depth (increasing temperature) following isothermal holding.

5.2.2. Evolution of the HePRZ

The Durango model predicts that the PRZ will essentially stabilize during isothermal holding, with its shape on a plot of temperature versus apatite date primarily affected by the isothermal holding duration. In contrast, in the RDAMM the accumulation of radiation damage causes a monotonic increase in the He retentivity of the apatites, such that the PRZ will continually shift to higher temperatures. Fig. 6 illustrates that the PRZ predicted by the RDAAM for an apatite with 28 ppm eU is located at lower temperatures than the Durango model after 25 Ma of isothermal holding (Fig. 6A), is similar to Durango after

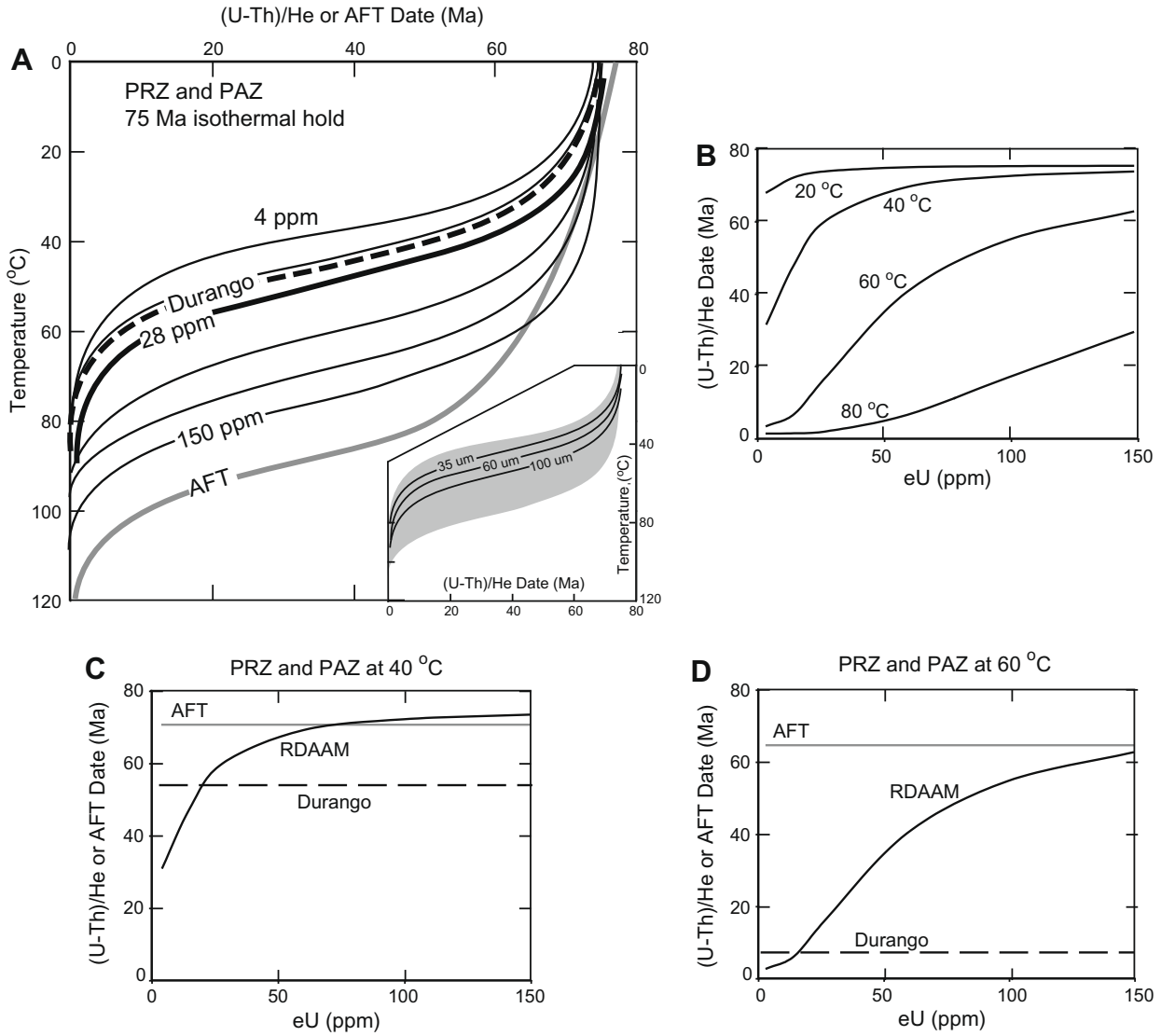

Fig. 5. (A) The helium partial retention zone (HePRZ) computed for apatites characterized by a range of eU using the RDAAM following 75 Ma of isothermal holding. Solid lines are for apatites with eU values of 4, 15, 60, 100, 150 ppm eU from top to bottom. Solid bold line is for apatite with typical 28 ppm eU value. The HePRZ computed using conventional Durango diffusion kinetics (bold dashed black line), and the AFT PAZ computed using Ketcham et al. (2007) apatite annealing kinetics (gray solid line) are depicted for comparison. The inset depicts the HePRZ for apatites characterized by radii varying from 35 to 100 μm and uniform 28 ppm eU (solid lines), and the variation in HePRZ predicted for eU from 4 to 150 ppm and uniform radius of 60 μm (gray shaded field). (B) Simulated (U–Th)/He date as a function of eU for the PRZ in (A) using the RDAAM at temperatures of 20, 40, 60, and 80 °C. (C) (U–Th)/He date as a function of eU for the PRZ in (A) at a temperature of 40 °C predicted using the RDAAM (solid black line) and Durango diffusion kinetics (dashed black line). AFT date as a function of eU for the PAZ in (A) is also shown (gray solid line). (D) Same as (C), but for a temperature of 60 °C.

75 Ma (Fig. 6B), and is at significantly higher temperatures after 500 Ma (Fig. 6C and D). The locations of the RDAAM PRZ curves relative to Durango are controlled by the magnitude of accumulated radiation damage in exactly the same manner as in Fig. 5A for different apatite eU values.

Fig. 7 shows how the predicted temperatures at the 90% point (top) and 10% point (bottom) of the PRZ change through time for the Durango model and for the RDAAM using a typical apatite eU value of 28 ppm. One consequence of this definition of the PRZ is that the temperature window depends on the holding duration. For the Durango model, both PRZ limits will move to cooler temperatures at longer holding times (Fig. 7). For the RDAAM, the ongoing accumulation of radiation damage is more important than this effect, such that the PRZ moves to higher temperatures for longer holding times. The bottom of the RDAAM PRZ eventually plateaus at ~80 °C, the temperature at which annealing keeps pace with production of damage and He diffusivity stops decreasing. After 500 Ma of isothermal holding even the base of the Durango PRZ resides above the top of the RDAAM PRZ (Fig. 7).

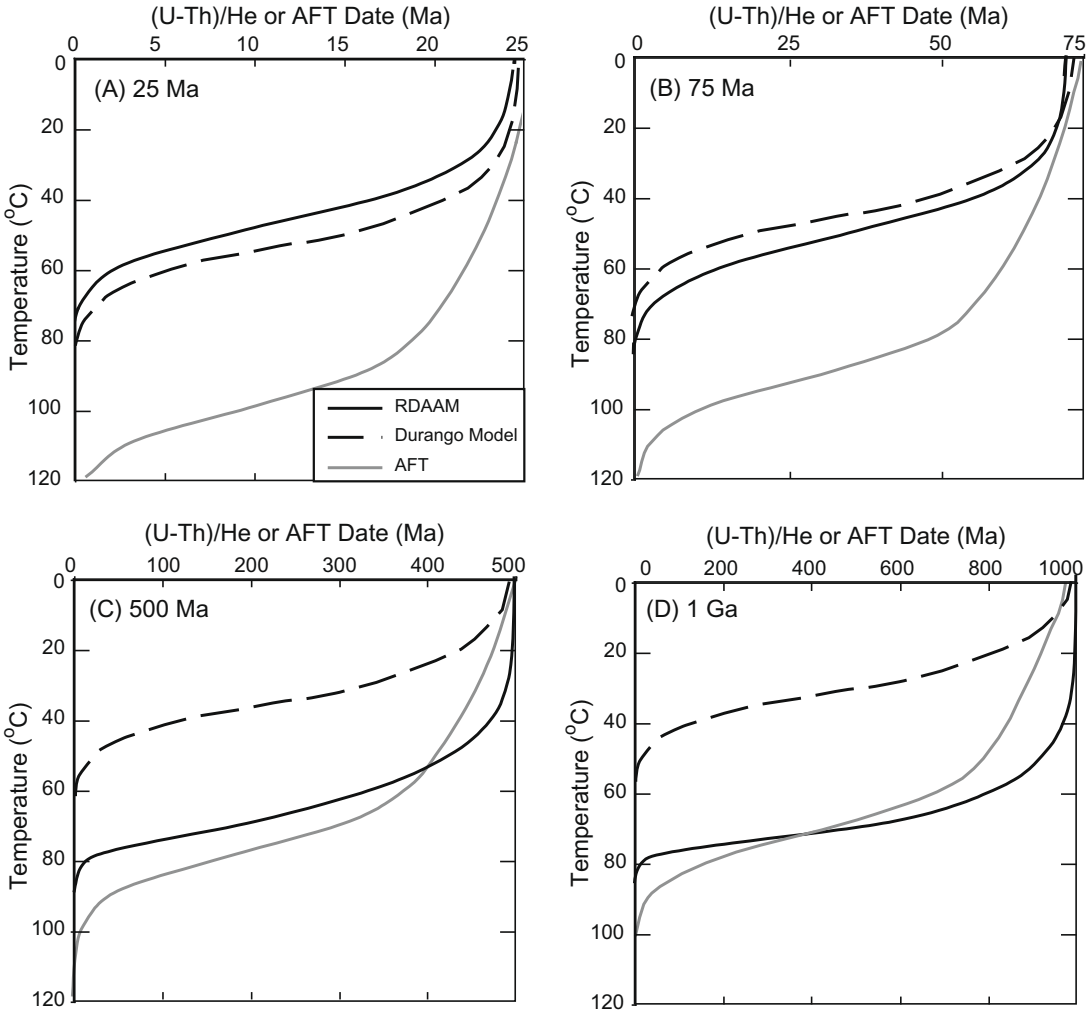

Fig. 6. The helium PRZ and AFT PAZ following (A) 25 Ma, (B) 75 Ma, (C) 500 Ma and (D) 1 Ga of isothermal holding. Curves are for the PRZ computed using the RDAAM for an apatite with a typical 28 ppm eU value (solid black line), for the PRZ computed using conventional Durango diffusion kinetics (dashed black line), and the PAZ using Ketcham et al. (2007) apatite annealing kinetics (solid gray line).

5.2.3. Inversions of (U–Th)/He and AFT dates and testable predictions of the RDAAM

An important result apparent from Figs. 5 and 6 is that apatites in the RDAAM PRZ may have older (U–Th)/He dates than corresponding AFT dates (Fig. 5A and C); this occurs when the PRZ plots at higher temperatures than the corresponding apatite fission-track partial annealing zone (PAZ, Fitzgerald and Gleadow, 1990). For a 75 Ma isothermal holding duration, this "age inversion" is predicted only for the highest eU apatites (100–150 ppm) and only at temperatures from ~30 to 55 °C (Fig. 5A, C, and D). For longer isothermal holding durations, apatites with more typical eU values are expected to show the effect. For example, after 500 Ma of isothermal holding, 28 ppm eU apatites in the temperature range from ~10 to 50 °C are predicted to have up to a 35 Ma inversion of (U–Th)/He and AFT dates (Fig. 6C). This temperature range corresponds to a ~2 km depth interval of the PRZ, assuming a geothermal gradient of 20 °C/km. For a 1 Ga holding time, there is an increase in the maximum magnitude (~125 Ma), temperature range (10–65 °C), and corresponding depth range (2.75 km) of the inversion for typical eU apatites (Fig. 6D).

The RDAAM simulations of the PRZ make three predictions that could be tested with samples from thermally stable boreholes with a known temperature gradient. First, the most readily testable prediction is that samples from a given depth in such a borehole should yield a range of (U–Th)/He dates correlated with eU. Following 75 Ma of isothermal holding at 60 °C, the ~60 Ma range in dates of apatites spanning 100 ppm eU would be easily detectable (Fig. 5B). Second, for extended isothermal holding durations (several hundred million years), the PRZ for typical eU apatites should be displaced to significantly higher temperatures than predicted by the Durango model (Fig. 7). Finally, an inversion of AFT and (U–Th)/He dates should be observed at 20–50 °C temperatures for typical eU apatites if isothermal holding was of sufficient duration (e.g., 500–1000 Ma), or for high eU apatites (100–150 ppm eU) for shorter holding durations (e.g., 75 Ma). It may be challenging, however, to convincingly identify a geologic environ-

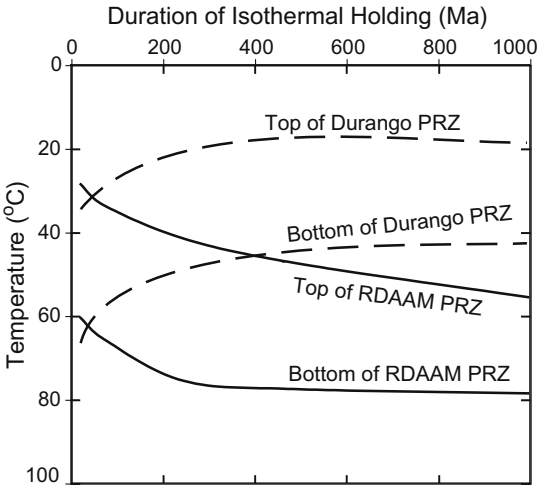

Fig. 7. Evolution of the temperature at the top and bottom of the PRZ as a function of the isothermal holding duration computed using the RDAAM (solid lines) and conventional Durango diffusion kinetics (dashed lines).

ment to undertake the latter two tests with apatite suites characterized by a sufficient eU range. There are likely to be few if any locations, even in stable cratonic regions, that can be proven to have experienced isothermal histories for hundreds of Ma without superimposed phases of reheating and cooling. Although shorter isothermal holding durations are probably more common, the corresponding effects become smaller.

5.3. Reheating during burial

5.3.1. Characteristics of apatite suites affected by partial He loss during reheating

The consequences of radiation damage on (U–Th)/He dates will be particularly significant for thermal histories involving an extended period of low temperature accumulation of helium and radiation damage followed by reheating and partial helium loss. To illustrate this effect, we simulated thermal histories characterized by a period of residence at the Earth's surface, followed by monotonic heating to some peak temperature, followed by monotonic cooling back to the Earth's surface. This scenario might apply to a cratonic region experiencing a period of burial followed by erosional unroofing. The particular history we modeled involved residence at 0 °C from 550 to 400 Ma, a peak temperature between 0 and 120 °C at 275 Ma, and cooling back to 0 °C by 150 Ma (Fig. 8A, upper right inset).

Fig. 8A shows the results for apatites with a range of eU values subjected to different maximum temperatures during the reheating step. At peak temperatures below ~30 °C, uniform dates are predicted because the temperatures are insufficient to induce He loss from any of the apatites. For peak reheating temperatures from ~30 to 100 °C, the model predicts that dates will be highly variable and positively correlated with eU (Fig. 8A and B). For example, at 80 °C peak reheating, apatites characterized by the lowest eU and least radiation damage will lose most of their He and so will yield the youngest dates (Fig. 8B). With increasing eU, He retentivities increase and He loss at this temperature decreases; at the highest eU He retentivities are high enough that apatites are almost unaffected by He loss and thus yield the oldest dates. Peak temperatures above ~110 °C are hot enough to induce complete He loss from all the apatites, and so yield a fairly uniform distribution of dates regardless of eU. Fig. 8B shows that the strength and shape of the correlation between eU and date is very sensitive to the peak temperature. The lower left inset in Fig. 8A compares the grain-size effect for apatites of 35–100 μm radius and 28 ppm eU with the results predicted by RDAAM for a 4–150 ppm eU span and uniform 60 μm half-width (gray shaded field). Although the grain-size effect is evident, it is clear that eU has greater influence for these thermal histories.

An important result of the thermal history simulations characterized by partial resetting shown in Fig. 8 is that the RDAAM predicts dates older than those using the Durango model for all apatites characterized by eU values greater than ~4 ppm (Fig. 8A,C,D). For example, for a peak reheating temperature of 80 °C, the RDAAM predicts that an apatite with 28 ppm eU will yield dates ~210 Ma older than those predicted by the Durango model. Thus, the use of a damage accumulation and annealing model is important for accurate interpretation of (U–Th)/He datasets that record thermal histories involving reheating and partial resetting.

5.3.2. Importance of duration at near-surface temperatures prior to reheating

The duration of residence at surface temperatures prior to reheating will also have a significant influence on the results of these simulations. Apatites that spent longer time at low temperatures will accumulate more radiation damage prior to reheating and so will be more retentive than apatites with the same eU that spent shorter time at low temperatures. This effect is depicted in Fig. 9 for an apatite with the typical 28 ppm eU value. Simulated thermal histories are the same as in Fig. 8, but the initial duration at 0 °C is allowed to vary from 0 Ma (Fig. 9A) to 300 Ma (Fig. 9B). In this example, the reheating temperatures required to induce a 25% reduction in the He date are 74 and 89 °C for the 0 and 300 Ma surface durations, respectively. By comparing Fig. 9A and B, it is also apparent that apatites that undergo longer initial durations of damage accumulation yield dates that increasingly deviate from the predictions of the Durango model. For the 0 Ma initial surface duration, to induce a 25% reduction in (U–Th)/He date the RDAAM requires a peak temperature 22 °C hotter than the Durango model. In contrast, for the 300 Ma of initial surface residence, the same 25% reduction in (U–Th)/He date requires a temperature 45 °C hotter than the Durango model.

These results have several important implications. First, when simulating a detrital apatite population, the (U–Th)/He provenance date, AHe_{dep}, must be considered. Fig. 9C depicts the results for the same thermal history as in Fig. 8, with a peak temperature of 80 °C, for apatites with a range of AHe_{dep} from 0–150 Ma (assumed to correspond

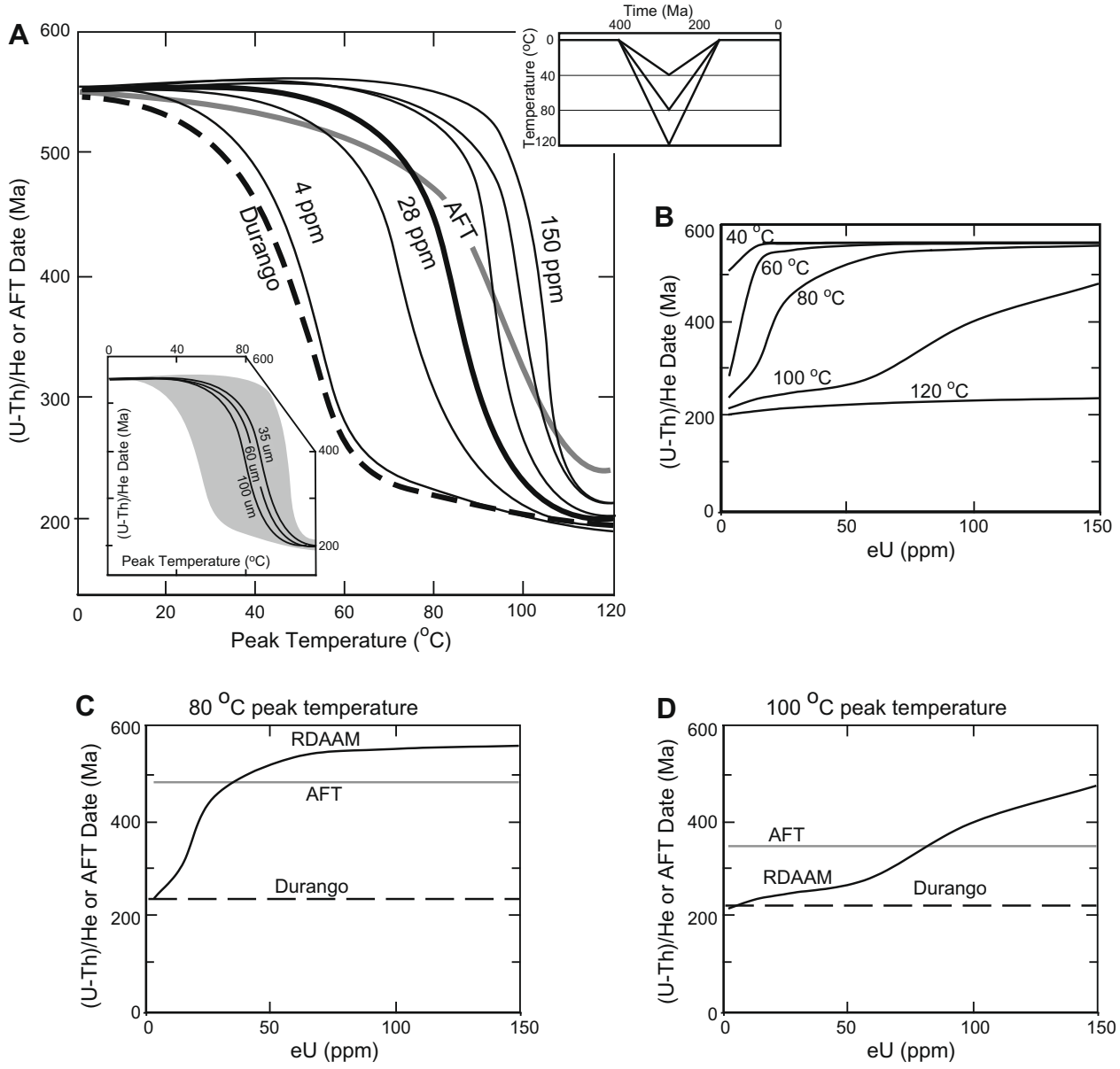

Fig. 8. (A) The effects of reheating on (U–Th)/He dates computed for apatites characterized by a range of eU using the RDAAM for different peak temperatures for the thermal history in the upper right inset. Solid black lines are for apatites with eU values of 4, 15, 60, 100, and 150 ppm from left to right. Solid bold line is for apatite with typical 28 ppm eU value. Results computed using conventional Durango diffusion kinetics (bold black dashed line) and for the AFT system using Ketcham et al. (2007) annealing kinetics (gray line) are also shown. The lower right inset depicts the results for apatites characterized by radii varying from 35 to 100 μm and uniform 28 ppm eU (solid lines), and the variation in results predicted for eU from 4 to 150 ppm and uniform radius of 60 μm (gray shaded field). (B) (U–Th)/He date versus eU for different peak temperature conditions of 40, 60, 80, 100, and 120 °C. (C) (U–Th)/He date as a function of eU at a peak temperature of 80 °C computed using the RDAAM (solid black line) and Durango diffusion kinetics (dashed black line). AFT date as a function of eU (solid gray line) is also depicted. (D) Same as (C), but for a peak temperature of 100 °C.

to holding at 0 °C). The simulations predict a fan of dates shown by the gray shading, with the upper and lower bounds representing AHe_{dep} values of 150 and 0 Ma, respectively. The fan of dates reflects the varying retentivities of the apatite population, as well as the spectrum of provenance dates. Second, these results highlight the importance of considering the duration at near-surface conditions prior to reheating. Varying this duration in thermal history simulations will affect the peak temperatures necessary to explain a (U–Th)/He dataset. Geological examples of (U–Th)/He datasets for both of these scenarios are provided below.

5.3.3. Inversions of (U–Th)/He and AFT dates

Like in the monotonic cooling and PRZ simulations, the RDAAM predicts that reheating during burial can induce

(U–Th)/He dates that are older, in some cases much older, than AFT dates. For the thermal histories simulated in Fig. 8, a typical 28 ppm eU apatite is predicted to yield inverted dates for peak reheating temperatures from 40 to 70 °C. The range of peak temperatures over which inversion of dates occurs increases for higher eU apatites. This range is 40–110 °C for the 150 ppm eU apatites simulated in Fig. 8, with a maximum inversion of dates of ~125 Ma. Similarly, longer initial durations of damage accumulation

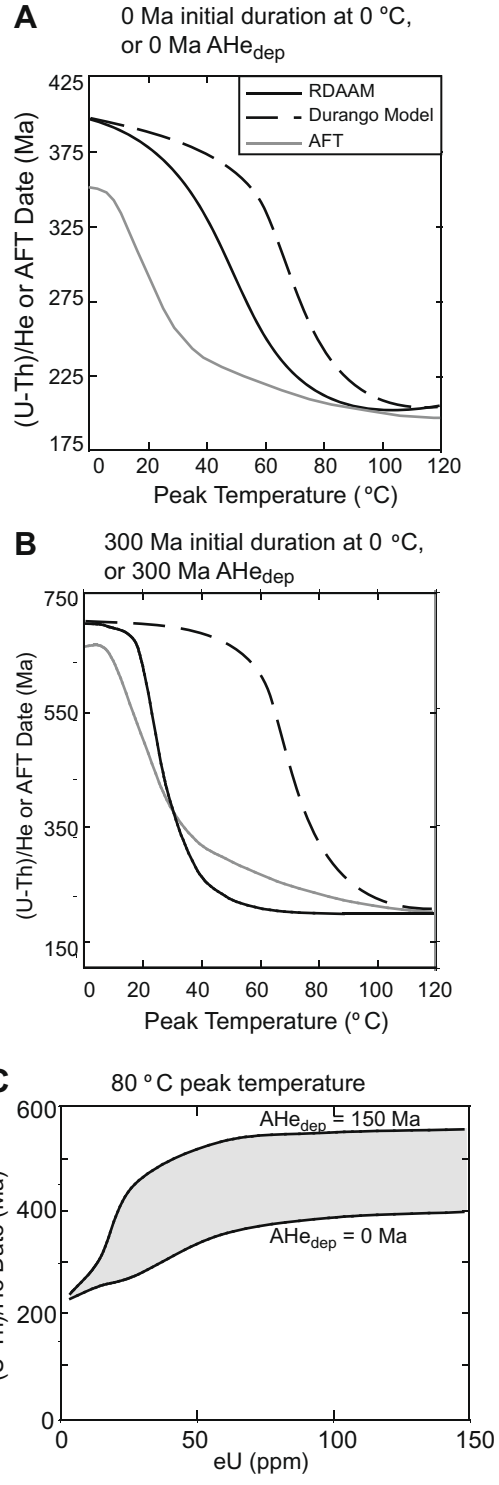

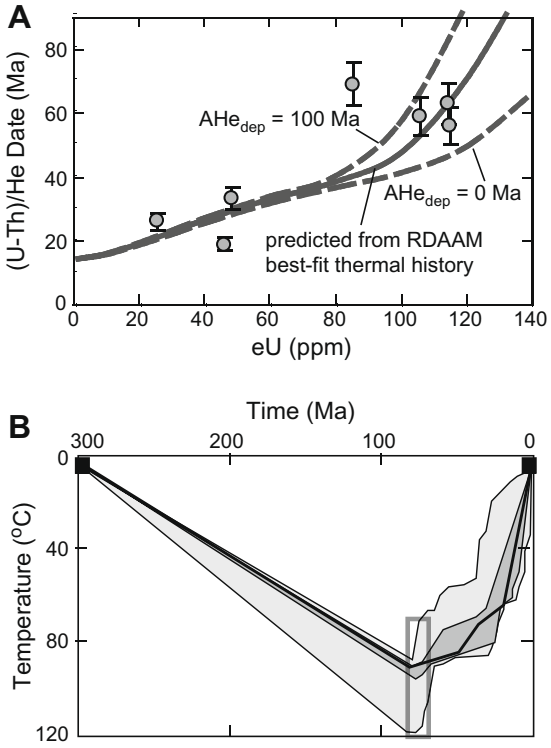

Fig. 10. (A) Individual apatite (U–Th)/He dates as a function of apatite eU for an Esplanade sandstone sample from the Grand Canyon region of the Colorado Plateau, from Flowers et al. (2007). Analytical errors are plotted at 8% (2-sigma). The predicted date-eU correlation for the best-fit thermal history in (B) is shown as the solid gray line. The dashed gray lines show the date-eU correlation for the same best-fit thermal history, but varying AHe$_{dep}$ from 0 to 100 Ma. (B) Inverse modeling results using the RDAAM. The constraints imposed on the thermal history are indicated by the two black squares at 300 and 0 Ma and the rectangular box at 80–70 Ma. A range of AHe$_{dep}$ from 0 to 100 Ma at 0–5 °C is assumed. The good-fit field of solutions is shown by the darker gray shading, and the acceptable-fit field in lighter gray shading. The solid black line represents the best-fit thermal history, with AHe$_{dep}$ of 14 Ma. The results are consistent with other geological and thermochronological constraints in the region.

Fig. 9. The effects of reheating on (U–Th)/He dates computed for different peak temperatures for the thermal history in the inset of Fig. 8A, for (A) 0 Ma initial duration at 0 °C, or AHe$_{dep}$ of 0 Ma, and (B) 300 Ma initial duration at 0 °C, or AHe$_{dep}$ of 300 Ma. Solid black lines are computed using the RDAAM for apatites with a typical 28 ppm eU value. Results computed using Durango diffusion kinetics (dashed black lines) and for the AFT system using Ketcham et al. (2007) annealing kinetics (gray lines) are also shown. (C) (U–Th)/He date as a function of eU computed using the RDAAM assuming a 0–150 Ma range of AHe$_{dep}$ (corresponding to holding at 0 °C) for a peak temperature of 80 °C for the thermal history in the inset of Fig. 8A. The gray shaded region represents the spectrum of dates predicted for this scenario, reflecting the differing retentivities of the apatites and the range of provenance dates.

at 0 °C increase the range of peak reheating temperatures predicted to cause inversions of dates. A 28 ppm eU apatite with 300 Ma of initial damage accumulation is predicted to yield inverted dates for peak reheating temperatures from 30 to 90 °C, with a maximum reversal of ~ 65 Ma.

5.3.4. Testable predictions of the RDAAM and examples from geological datasets

The RDAAM makes two testable predictions for low-temperature thermochronometry data from regions that underwent burial followed by unroofing. First, for a fairly broad range of peak temperatures the model predicts a positive correlation between (U–Th)/He date and eU. Second, under certain circumstances, the model predicts (U–Th)/He dates that are older than the fission-track dates for the same crystals. Here we briefly describe several datasets that are consistent with these predictions.

Colorado Plateau. Fig. 10A shows previously published (U–Th)/He dates for individual detrital apatite grains from a sample of Esplanade sandstone in the Grand Canyon region of the Colorado Plateau (Flowers et al., 2007). This suite includes apatites that span a large range in eU, which is positively correlated with a factor of ~3 range in He dates. Fig. 10B shows the inverse modeling results of HeFTy for this suite of apatites using the RDAAM, applying reasonable geological constraints, and assuming a 0–100 Ma duration at 0–5 °C prior to burial to approximate the range of (U–Th)/He dates when the apatites were deposited. The results of the thermal history simulations indicate partial to complete He loss from the apatites at peak temperatures, followed by multiphase cooling, in agreement with previous simulations using the HeTM (Flowers et al., 2007). The multiphase cooling path is consistent with that inferred from (U–Th)/He data (Fig. 4) and AFT track-length data (Kelley et al., 2001) for Grand Canyon basement samples deeper in the section.

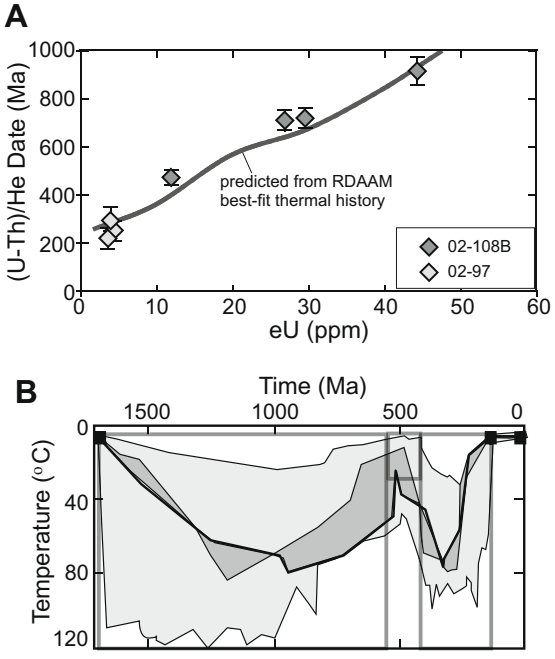

Fig. 11. (A) Individual apatite (U–Th)/He dates as a function of apatite eU for two Precambrian basement samples from the Canadian Shield, from Flowers (2009). Analytical errors are plotted at 2-sigma, propagated from the U, Th, and He measurement uncertainties and grain-length measurement uncertainties. The predicted date-eU correlation for the best-fit thermal history in (B) is shown as the solid gray line. (B) Inverse modeling results using the RDAAM. The constraints imposed on the thermal history are indicated by the three black squares and three rectangular boxes. The good-fit field of solutions is shown by the darker gray shading, and the acceptable-fit field in lighter gray shading. The solid black line represents the best-fit thermal history. The results are compatible with AFT data from the same area.

Canadian Shield. Four pairs of samples collected from the same outcrop or nearby outcrops in the Canadian Shield show eU correlations (Flowers, 2009). Fig. 11 presents the results for one of these sample pairs, in which (U–Th)/He dates for individual apatites show a nearly 600 Ma span of dates positively correlated with a ~40 ppm range in eU. Fig. 11B shows the inverse modeling results for these samples using the RDAAM, with thermal history constraints derived from regional unconformities. The thermal history from ca. 1.7 to ca. 550 Ma is unconstrained, and is included in the simulations to account for the effects of radiation damage accumulation prior to reheating. The key result is that the data require a phase of partial to complete He loss during reburial in Paleozoic to early Mesozoic time. AFT and track-length data from these samples (Flowers, 2009) and AFT studies elsewhere in the Canadian Shield similarly imply a reheating phase during this time interval (Crowley and Kuhlman, 1988; Osadetz et al., 2002).

Southeast Australia. Green et al. (2006) report a dataset from Early Cretaceous sediments of the Otway Basin, Australia, in which a correlation between apatite date and eU was qualitatively attributed to the effects of radiation damage on He diffusivity during burial and unroofing. (U–Th)/He dates for higher eU (mean 30 ppm) apatites extracted from a granite pebble yielded a mean date and standard deviation of 125 ± 18 Ma. (U–Th)/He dates of the low eU apatites (mean 8 ppm) of an adjacent sandstone are somewhat scattered, likely due to a combination of eU and grain-size variation, but are younger. Their mean date and standard deviation is 58 ± 21 Ma. Extensive thermochronological study of the Otway Group sediments, including AFT and vitrinite reflectance analysis, lead Green et al. (2006) to favor a thermal history characterized by two phases of reheating and cooling, in mid-Cretaceous and late Miocene time. Here we test whether the RDAAM can reproduce the mean (U–Th)/He dates for the granite cobble and sandstone samples with thermal history constraints based on those derived from the previous thermochronological studies. The simulations begin at 125 Ma during coeval volcanism and deposition of the predominantly volcaniclastic sediments. We assume the 20 °C surface temperature used by Green et al. (2006) for direct comparison with the results of the AFT thermal history simulations. Fig. 12 shows the inverse modeling results for the (U–Th)/He data. Green et al.'s (2006) "best-fit" thermal history solution for

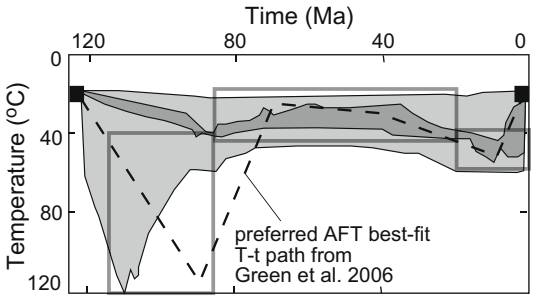

Fig. 12. Inverse modeling results using the RDAAM for Otway Basin (U–Th)/He data of Green et al. (2006) for granite cobble and sandstone samples. The constraints imposed on the thermal history are indicated by the two black squares and three rectangular boxes. The good-fit field of solutions based on the He data using the RDAAM is shown as the dark gray shading, and the acceptable-fit field in lighter gray shading. The dashed black line represents Green et al.'s (2006) preferred best-fit thermal history results based on AFT data for the granite cobble. The RDAAM inverse modeling results are in good agreement with the constraints derived independently from the AFT and other data.

AFT data from the granite cobble is shown as the black dashed line for reference. Thus, the (U–Th)/He data interpreted using RDAAM are in good agreement with AFT data from one of the same samples, as well as with other independent constraints.

Other localities. The RDAAM may explain enigmatic data in which (U–Th)/He dates are older than predicted based on AFT dates or other geological constraints from the same area, or are actually older than the corresponding AFT dates themselves. Thermochronometry data from southern East Greenland (Hansen and Reiners, 2006), the Yilgarn craton in Australia (Green et al., 2006), and the Bighorn Mountains in Wyoming (Crowley et al., 2002) are examples of the former. (U–Th)/He dates older than corresponding AFT dates are present in datasets from the Lake Mountain rhyodacite in Australia (Green et al., 2006), Precambrian basement in West Greenland (Green et al., 2006), cratonic basement in Sweden (Hendriks and Redfield, 2005), and the Blue Ridge escarpment in the eastern United States (Spotila et al., 2004). There is insufficient eU spread in these datasets to determine if a correlation between (U–Th)/He date and eU is present. In all of these examples, reheating and cooling during burial and unroofing are inferred as a portion of the thermal history, although in at least one case (Hendriks and Redfield, 2005) this interpretation is controversial. As described above, the simulations using the RDAAM predict that (U–Th)/He and AFT age reversals are likely to be most common, and have the potential to be most clearly documented, in apatite suites that experienced such reheating and cooling histories. It is likely that the RDAAM will help reconcile the discrepancies between the (U–Th)/He and AFT results in some of these reported datasets.

6. CONCLUSIONS

The new RDAAM kinetic model tracks the evolution of He retentivity in apatite by accounting for both the accumulation and the annealing of radiation damage. This new model differs from the Shuster et al. (2006) radiation damage trapping model in that it uses effective fission-track density, rather than He concentration, as the proxy for the volume fraction of radiation damage.

Simulations of common thermal histories using the RDAAM reveal several significant and testable predictions that differ from those using the conventional Durango model in which the apatite He diffusion kinetics are constant through time. First, for common thermal histories, the RDAAM predicts distinctive nonlinear positive correlations between apatite (U–Th)/He date and apatite eU for apatite suites with a large eU span. Second, the RDAAM commonly predicts significantly older (U–Th)/He dates than previously expected from Durango kinetics; in some cases these predicted dates are older than their corresponding AFT dates. Notable consequences of the RDAAM for specific thermal history simulations include (1) effective closure temperatures that increase with decreasing cooling rates, rather than decreasing as predicted by the Dodson (1973) formulation of closure temperature, (2) a HePRZ that continuously evolves to higher temperatures, such that for sufficient holding times it will no longer overlap the PRZ predicted by the Durango model, and (3) burial and reheating scenarios that yield a several hundred Ma span of dates for apatites characterized by large eU variation.

The RDAAM can quantitatively explain four previously published datasets that show date-eU correlations from three different locations (Colorado Plateau, Canadian Shield, southeast Australia) using geologically reasonable thermal histories consistent with independent evidence. In addition, the RDAAM will likely help resolve some previously reported disparities between (U–Th)/He and AFT results, including those in which the (U–Th)/He date is older than the corresponding AFT date. We caution, however, that complicating factors such as He implantation from external phases, microinclusions with high eU, and fluid inclusions can induce anomalously old (U–Th)/He dates and/or scatter in the data that are unrelated to enhanced He retention associated with radiation damage accumulation. In these particular cases, a negative date-eU correlation may be displayed that can help identify these effects, owing to a proportionately greater influence of the excess He on the date of the lower eU apatites. Short-duration reheating of samples may also induce (U–Th)/He and AFT age reversals that are not linked with the radiation damage effect (e.g., Stockli et al., 2000; Reiners et al., 2007).

The RDAAM is sensitive to the kinetics of annealing at low temperatures, over which there remains substantial controversy in the fission-track community (e.g., Hendriks and Redfield, 2005). These effects are especially important for old samples, and it is probable that the RDAAM will not reconcile all discrepancies between the (U–Th)/He and AFT methods. A new or different annealing model could be adopted in HeFTy to govern the generation and elimination of radiation damage in the RDAAM, and would not affect the primary RDAAM calibration of He diffusion and effective fission-track density data.

ACKNOWLEDGMENTS

This work was supported by National Science Foundation Grants EAR-0738627 to K.A.F., EAR-0738474 to D.L.S., and EAR-0711451 to R.M.F. D.L.S. acknowledges support from the Ann and Gordon Getty Foundation. We thank Ray Donelick for supplying many of the apatite fission-track density measurements that are used in the model calibration. We appreciate helpful reviews by Pete Reiners and an anonymous reviewer.

APPENDIX A. SUPPLEMENTARY DATA

Supplementary data associated with this article can be found, in the online version, at doi:10.1016/j.gca.2009.01.015.

REFERENCES

Carlson W. D., Donelick R. A. and Ketcham R. A. (1999) Variability of apatite fission-track annealing kinetics: I. Experimental results. *Am. Mineral.* **84**, 1213–1223.

Crowley K. D. and Kuhlman S. L. (1988) Apatite thermochronometry of western Canadian Shield: implications for origin of the Williston Basin. *Geophys. Res. Lett.* **15**, 221–224.

Crowley P. D., Reiners P. W., Reuter J. M. and Kaye G. D. (2002) Laramide exhumation of the Bighorn Mountains, Wyoming: an apatite (U–Th)/He thermochronology study. *Geology* **30**, 27–30.

Damon P. E. and Kulp J. L. (1957) Determination of radiogenic helium in zircon by stable isotope dilution technique. *Trans. Am. Geophys. Union* **38**, 945–953.

Dodson M. H. (1973) Closure temperatures in cooling geological and petrological systems. *Contrib. Mineral. Petrol.* **40**, 259–274.

Dumitru R. A., Duddy I. R. and Green P. F. (1994) Mesozoic-Cenozoic burial, uplift and erosion history of the west-central Colorado Plateau. *Geology* **22**, 499–502.

Farley K. A. (2000) Helium diffusion from apatite: general behavior as illustrated by Durango fluorapatite. *J. Geophys. Res.* **105**, 2903–2914.

Fitzgerald P. and Gleadow A. J. W. (1990) New approaches in fission-track geochronology as a tectonic tool: examples from the Transantarctic Mountains. *Nucl. Tracks Radiat. Meas.* **17**, 351–357.

Fleischer R. L. (2003) Etching of recoil tracks in solids. *Geochim. Cosmochim. Acta* **67**, 4769–4774.

Flowers R. M., Shuster D. L., Wernicke B. P. and Farley K. A. (2007) Radiation damage control on apatite (U–Th)/He dates from the Grand Canyon region, Colorado Plateau. *Geology* **35**, 447–450.

Flowers R. M., Wernicke B. P. and Farley K. A. (2008) Unroofing, incision and uplift history of the southwestern Colorado Plateau from apatite (U–Th)/He thermochronometry. *Geol. Soc. Am. Bull.* **120**, 571–587.

Flowers R. M. (2009) Exploiting radiation damage control on apatite (U–Th)/He dates in cratonic regions. *Earth Planet. Sci. Lett.* **277**, 148–155.

Galliker D., Hugentobler E. and Hahn B. (1970) Spontane Kernspaltung von ^{238}U und ^{241}Am. *Helv. Phys. Acta* **43**, 593–606.

Green P. F., Duddy I. R., Gleadow A. J. W., Tingate P. R. and Laslett G. M. (1986) Thermal annealing of fission tracks in apatite 1. A qualitative description. *Chem. Geol.* **59**, 237–253.

Green P. F., Crowhurst P. V., Duddy I. R., Japsen P. and Holford S. P. (2006) Conflicting (U–Th)/He and fission track ages in apatite: enhanced He retention, not anomalous annealing behavior. *Earth Planet. Sci. Lett.* **250**, 407–427.

Hansen K. and Reiners P. W. (2006) Low temperature thermochronology of the southern East Greenland continental margin: evidence from apatite (U–Th)/He and fission track analysis and implications for intermethod calibration. *Lithos* **92**, 117–136.

Hendriks B. W. H. and Redfield T. F. (2005) Apatite fission track and (U–Th)/He data from Fennoscandia: an example of underestimation of fission track annealing in apatite. *Earth Planet. Sci. Lett.* **236**, 443–458.

Hurley P. M. (1952) Alpha ionization damage as a cause of low helium ratios. *Trans. Am. Geophys. Union* **33**, 174–183.

Jonckheere R. and Van Den Haute P. (1996) Observations on the geometry of etched fission tracks in apatite: implications for models of track revelation. *Am. Mineral.* **81**, 1476–1493.

Jonckheere R. and Van Den Haute P. (2002) On the efficiency of fission-track counts in an internal and external apatite surface and in a muscovite external detector. *Rad. Meas.* **35**, 29–40.

Jonckheere R. (2003) On methodical problems in estimating geological temperature and time from measurements of fission tracks in apatite. *Rad. Meas.* **36**, 43–55.

Kelley S. A., Chapin C. E. and Karlstrom K. E. (2001) Laramide cooling history of Grand Canyon, Arizona, and the Front Range, Colorado, determined from apatite fission-track thermochronology. In *Colorado River Origin and Evolution* (eds. R. A. Young and E. E. Spamer). Grand Canyon Association, Grand Canyon National Park, Grand Canyon, Arizona, pp. 37–42.

Ketcham R. A., Donelick R. A. and Carlson W. D. (1999) Variability of apatite fission-track annealing kinetics: extrapolation to geological time scales. *Am. Mineral.* **84**, 1235–1255.

Ketcham R. A. (2003) Observations on the relationship between crystallographic orientation and biasing in apatite fission-track measurements. *Am. Mineral.* **88**, 817–829.

Ketcham R. A., Donelick R. A. and Donelick M. B. (2003) AFTSolve: a program for multi-kinetic modeling of apatite fission-track data. *Am. Mineral.* **88**, 929.

Ketcham R. (2005) Forward and inverse modeling of low temperature thermochronometry data. In *Thermochronology. Rev. Min. Geochem* 58 (eds. P. W. Reiners and T. A. Ehlers) pp. 275–314.

Ketcham R. A., Carter A. C., Donelick R. A., Barbarand J. and Hurford A. J. (2007) Improved modeling of fission-track annealing in apatite. *Am. Mineral.* **92**, 799–810.

Naeser C. W., Duddy I. R., Elston D. P., Dumitru T. A. and Green P. F. (1989) Fission-track dating: ages of Cambrian strata and Laramide and post-middle Eocene cooling events from the Grand Canyon, Arizona. In *Geology of the Grand Canyon, Northern Arizona* (ed. D. P. Elston et al.). Am. Geophys. Union, Washington, DC, pp. 139–144.

Osadetz K. G., Kohn B. P., Feinstein S. and O'Sullivan P. B. (2002) Thermal history of Canadian Williston basin from apatite fission-track thermochronology—implications for petroleum systems and geodynamic history. *Tectonophysics* **349**, 221–249.

Reiners P. W. and Farley K. A. (2001) Influence of crystal size on apatite (U–Th)/He thermochronology: an example from the Bighorn Mountains, Wyoming. *Earth Planet. Sci. Lett.* **188**, 413–420.

Reiners P. W., Thomson S. N., McPhilips D., Donelick R. A. and Roering J. J. (2007) Wildfire thermochronology and the fate and transport of apatite in hillslope and fluvial environments. *J. Geophys. Res.* **112**, F04001.

Shuster D. L. and Farley K. A. (2009) The influence of artificial radiation damage and thermal annealing on helium diffusion kinetics in apatite. *Geochim. Cosmochim. Acta* **73**, 183–196.

Shuster D. L., Flowers R. M. and Farley K. A. (2006) The influence of natural radiation damage on helium diffusion kinetics in apatite. *Earth Planet. Sci. Lett.* **249**, 148–161.

Spotila J. A., Bank G. C., Reiners P. W., Naeser C. W., Naeser N. D. and Henika B. S. (2004) Origin of the Blue Ridge escarpment along the passive margin of eastern North America. *Basin Res.* **16**, 41–63.

Stockli D. F., Farley K. A. and Dumitru T. A. (2000) Calibration of the apatite (U–Th)/He thermochronometer on an exhumed fault flock, White Mountains. *Geology* **28**, 983–986.

Warnock A. C., Zeitler P. K., Wolf R. A. and Bergman S. C. (1997) An evaluation of low-temperature apatite U–Th/He thermochronometry. *Geochim. Cosmochim. Acta* **61**, 5371–5377.

Wolf R. W., Farley K. A. and Silver L. T. (1996) Helium diffusion and low temperature thermochronometry of apatite. *Geochim. Cosmochim. Acta* **60**, 4231–4240.

Wolf R. A., Farley K. A. and Kass D. M. (1998) Modeling of the temperature sensitivity of the apatite (U-Th)/He thermochronometer. *Chemical Geology* **148**, 105–114.

Zeitler P. K., Herczig A. L., McDougall I. and Honda M. (1987) U–Th-He dating of apatite: a potential thermochronometer. *Geochim. Cosmochim. Acta* **51**, 2865–2868.

Associate editor: Rainer Wieler